HHS Public Access

Author manuscript

J Microsc. Author manuscript; available in PMC 2019 May 01.

Published in final edited form as:

J Microsc. 2018 May ; 270(2): 142–149. doi:10.1111/jmi.12667.

High-performance serial block-face SEM of non-conductive biological samples enabled by focal gas injection-based charge compensation

Thomas J. Deerinck[1], **Tristan Shone**[1], **Eric A. Bushong**[1], **Ranjan Ramachandra**[1], **Steven T. Peltier**[1], and **Mark H. Ellisman**[1,2,3,4]

[1]Center for Research in Biological Systems and the National Center for Microscopy and Imaging Research, University of California, San Diego, La Jolla, CA, USA

[2]Department of Neurosciences, University of California at San Diego, La Jolla, San Diego, California 92093, USA

[3]Salk Institute for Biological Studies, La Jolla, California 92037, USA

[4]Howard Hughes Medical Institutes Janelia Research Campus, Ashburn, VA, USA

Summary

A longstanding limitation of imaging with serial block-face scanning electron microscopy is specimen surface charging. This charging is largely due to the difficulties in making biological specimens and the resins in which they are embedded sufficiently conductive. Local accumulation of charge on the specimen surface can result in poor image quality and distortions. Even minor charging can lead to misalignments between sequential images of the block-face due to image jitter. Typically, variable-pressure SEM is used to reduce specimen charging, but this results in a significant reduction to spatial resolution, signal-to-noise ratio and overall image quality. Here we show the development and application of a simple system that effectively mitigates specimen charging by using focal gas injection of nitrogen over the sample block-face during imaging. A standard gas injection valve is paired with a precisely positioned but retractable application nozzle, which is mechanically coupled to the reciprocating action of the serial block-face ultramicrotome. This system enables the application of nitrogen gas precisely over the block-face during imaging while allowing the specimen chamber to be maintained under high vacuum to maximize achievable SEM image resolution. The action of the ultramicrotome drives the nozzle retraction, automatically moving it away from the specimen area during the cutting cycle of the knife. The device described was added to a Gatan 3View system with minimal modifications, allowing high-resolution block-face imaging of even the most charge prone of epoxy-embedded biological samples.

Keywords

Scanning electron microscopy; serial block-face imaging; backscatter electron; 3View; specimen charging

Corresponding author: Dr. Mark H. Ellisman Department of Neurosciences University of California, San Diego School of Medicine, 1000 BSB 9500 Gilman Drive, MC0608 La Jolla, CA 92093-0608, USA mellisman@ncmir.ucsd.edu.

Introduction

Serial block-face scanning electron microscopy (SBEM), introduced by Leighton, and later substantially improved and refined by Denk and Horstmann, is revolutionizing biological electron microscopy by enabling the acquisition of 3-dimensional volume images of relatively large regions of cells and tissues at nanometer-scale resolution (Denk & Horstmann, 2004, Leighton, 1981). The instrument consists of an ultramicrotome fitted within a backscatter-detector equipped SEM, and in an automated process, the ultramicrotome removes an ultra-thin slice of the specimen block-face surface with a diamond knife and the region of interest is imaged. This sequence is repeated hundreds or thousands of times until the desired volume of tissue is traversed.

This method enables the acquisition of thousands of cubic microns of imaging data with minimal operator involvement, and an SBEM platform based on the design of Denk and Horstmann is commercially available (Gatan 3View, Gatan Inc., Pleasanton, Ca).

Prior to imaging, specimens must be embedded in epoxy resin, which is non-conductive. When non-conductive specimens are imaged by SEM under high vacuum, some electrons that interact with the specimen cannot dissipate. The resulting accumulation of charge leads to significant distortion of images as the electric field associated with the charging specimen interferes with the imaging beam. There are several methods for attempting to mitigate this issue in SBEM, most based on approaches typically taken when preparing and imaging biological specimens for SEM. Biological specimens are often coated with thin layers of metal, and this approach has been adapted for use with SBEM by installing a sputter coater within the microscope imaging chamber (Titze & Denk, 2013); however, this approach has not been widely adopted.

Another approach to mitigate charging is to surround the specimen with conductive silver impregnated epoxy (Wanner *et al.*, 2016). While this can be effective, it is not applicable to all tissues or with cultured cell monolayers, and it renders the specimen opaque to light, making correlated light and SBEM more difficult. Additionally, attempts to infiltrate epoxy resin with carbon (Nyugen *et al.*, 2016) have similar limitations with inhomogeneous carbon deposition and specimen opaqueness. A common approach used to prepare specimens for SEM imaging is conductive impregnation with heavy metal stains (Friedman & Ellisman, 1981, Murakami *et al.*, 1983). With the introduction of sequential intense heavy metal *en bloc* staining for SBEM, some types of specimens such as brain tissue can be imaged at high vacuum without charging and with a considerable improvement in image resolution (Deerinck *et al.*, 2010, Wilke *et al.*, 2013). Nevertheless, even with intense heavy metal staining, many specimens, especially those containing large regions of bare epoxy resin (e.g. lung tissue, cultured cell monolayers) or relatively low lipid content (muscle, bone, plant tissue), cannot be imaged at high vacuum without substantial specimen charging artifacts. The most commonly used approach to reducing charging in SBEM is variable pressure SEM (VP-SEM). While very effective at reducing specimen charging, VP-SEM results in a substantial degradation of image quality due electron scattering, especially at the low accelerating voltages preferred for block-face imaging (Griffin, 2007) that are used to reduce

the specimen sample excitation volume (depth) from which backscattered electron signals are retrieved (Bouwer *et al.*, 2017). There is also a significant reduction of signal-to-noise ratio (SNR) using VP-SEM, estimated to be greater than 70% when compared to high vacuum conditions (Titze & Denk, 2013). This is usually ameliorated by using longer pixel dwell times, increased primary beam energy and/or current, or all three, substantially affecting data acquisition rates and specimen cutability due to beam damage.

Here we demonstrate results obtained using a simple mechanical device that enables small amounts of nitrogen gas to be locally injected above the sample, providing a very effective charge compensation method we refer to as Focal CC (for *Focal Charge Compensation*). Focal CC introduces a gas in the immediate vicinity of the block-face, which effectively eliminates specimen charging but still allows for high-resolution imaging of charge-prone samples. We show that Focal CC significantly outperforms VP-SEM imaging and performs nearly as well as high-vacuum SEM, even when imaging extremely challenging specimens.

Materials and Methods

Specimen preparation

Cultured cells and tissues were prepared as previously described using a combination of glutaraldehyde fixation, ferrocyanide reduced osmium tetroxide post-fixation, thiocarbohydrazide and osmium tetroxide liganding, followed by *en bloc* uranyl acetate and lead aspartate staining (Deerinck *et al.*, 2010, Ngo *et al.*, 2016, Williams *et al.*, 2011). Cultured cells were also stained for DNA using click-chemistry as previously described (Ngo *et al.*, 2016). Briefly, HeLa cells were incubated overnight in media containing 10 micromolar 5-ethynyl-2′-deoxyuridine (EdU, Life Technologies) and the following day, copper-mediated click-chemistry (Click-iT Cell Reaction Kit, Invitrogen) was used to attach dibromofluorescein-azide (1 micromolar) to the EdU incorporated into cellular DNA during replication, which was then used to photooxidize diaminobenzidine into a reaction product prior to treatment with osmium tetroxide (Ngo et al., 2016). Cultured cells were also prepared using a genetically targeted ascorbate peroxidase in order to stain the endomembrane system (Martell *et al.*, 2012). Epoxy embedded samples were mounted to aluminum pins (Gatan) using either silver epoxy (Ted Pella, Redding CA) or cyanoacrylic adhesive, or mounted on a custom designed tip-tilt holder and sputter coated with a thin layer of Au/Pd prior to block-face imaging.

Serial block-face imaging

Serial block-face imaging was accomplished using a Gemini SEM 300 or Merlin SEM (Zeiss, Oberkochen, Germany) equipped with a Gatan 3View system (model: *3View2XP* or Gatan's earlier *3View* system, respectively) and a nitrogen gas injection manifold (Zeiss model 346061-9002-200), modified to prevent pneumatic insertion while retaining software control of gas injection and maintenance of chamber pressure. For this work, cells and tissues were typically imaged at 2.5 keV, using 50-70 nm cutting intervals, 2.0 nm pixel size, beam dwell time of 0.5-1 μsec and a high vacuum chamber pressure of ~5×10^{-3} mbar for gas injection, 0.3 mbar for variable chamber pressure imaging, or <5×10^{-6} mbar for high

vacuum only. Specimen beam current was measured using a standard Faraday cup and current monitor (Zeiss).

Preliminary tests demonstrated that to be effective, gas injection must occur less than 1 mm from the sample block-face and ideally as close as possible, as the charge compensation effect is highly localized due to the rapid dispersion of gas molecules. While the gas injection system monitors the overall chamber pressure and allows for pressures as high as 7×10^{-3} mbar, the exact pressure on the sample surface cannot be measured due to the rapid dispersion of the gas molecules. Because of limited clearance between the 3View ultramicrotome and BSE detector, as well as the requisite cutting cycle, the standard fixed needle gas injection delivery system supplied with the Zeiss 346061-9002-200 gas injection system could not be adapted. Instead, we designed a device that could focally deliver nitrogen gas during imaging, and allows for automatic retraction during block-face cutting (Fig. 1A,B), thereby avoiding interference with the mechanical components of the 3View knife. The assembly fabricated requires no physical alterations to the 3View system other than attaching to components of the ultramicrotome using existing screw holes that are normally used during initial system installation and alignment. It uses the normal motion of the 3View ultramicrotome to reposition the nozzle to the retracted state and includes a spring-driven mechanism to precisely reposition the nozzle above the sample after each 3View cut to provide charge compensation for the entire block-face area being imaged (Supp. Movie 1).

The assembly is comprised of three major components and several sub-components (including off-the-shelf standard fasteners, nuts, etc.), all parts were fabricated from 316 stainless steel unless otherwise noted. The first major component is a rotating arm (Fig. 1B.1), which allows for the mounting and retraction of the nozzle for focal gas delivery. The nozzle consists of a rigid needle (Fig. 1B.2), which is secured to a small ramped platform (Fig. 1B.3) via an ultralow-profile socket head screw. We found carbon fiber tubing (material: Toray T700 Composite with Bisphenol A Epoxy Resin, OD: 0.028 in, ID: 0.011 in, length: 0.315 in) to be an ideal material choice for the needle as it is durable, conductive, non-magnetic, and inexpensive. The nozzle is fastened via a second ultralow-profile socket head screw to the distal end of the primary arm. When this fastener is loosened, the nozzle can rotate, allowing the tip of the needle to be clocked relative to the sample to further tune its fixed orientation. The ramp of the platform angles the needle down and provides a sliding surface to allow the tip to be positioned very close to the sample block-face. The needle is connected to the Zeiss gas injection manifold using standard silicon tubing (OD: 0.060 in, ID: 0.020 in, WALL: 0.020 in) (Fig. 1B.4), which is routed along the length of the arm and away from other components within the chamber of the instrument. The arm is mounted to an existing tapped hole on the top of the 3View stage using a shoulder screw and brass bushing, which together comprise a simple bearing (Fig. 1B.5) about which the arm rotates. The rotation is actuated by the second major component of the assembly, an adjustable tappet (Fig. 1B.6) which is bolted to the forks of the SBEM knife assembly (using an existing tapped hole). The third major component of the assembly is a block (Fig. 1B.7), which provides a physical stop (Fig. 1B.8) for constraining the rotation of the cantilevered arm and ensuring the nozzle is returned exactly to its original position for gas injection. This block is also bolted to the 3View stage using an existing tapped hole. The position of the

physical stop can be adjusted via a finely threaded socket head screw and fixed in place with a knurled lock nut. This adjustment provides a second mechanism for precisely aligning the nozzle tip relative to the sample. An extension spring (Century Spring Corp., model N-175, material: music wire, OD: 0.109in, LENGTH: 0.500in, RATE: 0.080 lbs/in) completes the assembly. It connects the proximal end of the rotating arm to the block (Fig. 1B.9) and powers the return of the nozzle back to its primary position as the knife is cleared and the tappet is retracted.

Image Analysis

To calculate resolution, Fast Fourier Transforms (FFTs) were acquired at 3 different regions of each image for an ROI of 2048 × 2048 pixels each (Joy, *et al.*, 2000). To make the measurements consistent and unambiguous for all the different imaging conditions, the cut-off threshold to distinguish the signal from the noise in the FFT was set to ~20%. The measured resolution with a ~20% threshold cut-off may be pessimistic for images with high SNR, however, the purpose of this study is only to obtain the relative degradation of the resolution with the different imaging conditions, and not to make any claim about the absolute achievable resolution of the instrument. For each thresholded FFT, the resolution was measured in the ± X and ± Y directions (all 4 values would be the identical for a perfect stigmation-corrected image) and the average was obtained.

The SNR was obtained using the inverted SEM image, by dividing the signal by the standard deviation of the background intensity (He & Zhou, 2008, Waters, 2009). The signal was calculated by subtracting the mean intensity values of regions that had strong contrast from metal deposition (e.g., mitochondria) from the regions in the cytoplasm that had little contrast, representing the background intensity. The SNR was calculated from 3 different regions of the images, and the average was computed.

Histograms were generated using FIJI. For movies, raw and unaligned images were binned by 4 and stacked using Digital Micrograph (Gatan), saved as .avi and converted to .mov format using QuickTime (Apple Inc., Cupertino, CA). Volume reconstructions were made using raw and unaligned image stacks using blend projection thresholding using IMARIS (Bitplane, Concord, MA).

Results

To evaluate the performance of Focal CC on block-face imaging, we chose two common types of specimens known to be extremely charge-prone: lung tissue with alveoli, interstitial spaces and vasculature, and sparse cultured cell monolayers surrounded by bare resin. For these samples, it was impossible to obtain good images at 2.5 keV accelerating voltage and high vacuum due to massive specimen charging (Fig. 2A, C). The integrated gas injection software allows for routine imaging up to 7×10^{-3} mbar chamber pressure, but we found that focal gas injection resulting in a chamber pressure of $3\text{-}5\times10^{-3}$ mbar was sufficient to completely mitigate charging on these samples (Fig. 2B, D) if the gas injection needle was in immediate proximity to the block-face.

The gas injection system described does not interfere with the operation of the 3View system, and greatly reduces image jitter in volume stacks of even severely charge-prone samples such as lung tissue or sparse cell cultures (Supp. Movies 2-5, raw unaligned data). Additionally, since the overall chamber pressure is maintained under high vacuum ($<7\times10^{-3}$ mbar), ease of focusing and stigmation is comparable to high vacuum imaging without gas injection and far superior to what is required when using VP-SEM. Moreover, we found no need for focus or stigmation adjustment over the course of the volume acquisitions as the injection needle is returned precisely to the required position between each cutting-imaging cycle. This high degree of stability was tested and confirmed for a variety of conductive, non-magnetic needle materials, including carbon fiber, brass, and non-magnetic (316) stainless steel.

To assess image quality of Focal CC versus VP-SEM in charge-prone samples, cultured cells were imaged using both modes (80% N_2 injection and $\sim5 \times 10^{-3}$ mbar chamber pressure, Fig. 3A, and 0.3 mbar VP-SEM, Fig. 3B) at 2.5 keV and otherwise identical imaging parameters. The difference in contrast and resolution is easily discernable. Some residual charging is evident when imaging this sample by VP-SEM at 0.3 mbar chamber pressure (the maximum allowed with the Gemini SEM). A further benefit to this approach is that the beam boost system employed in the Gemini SEM can be used concurrently with gas injection, offering improved system stability at low accelerating voltages over long periods of time; a feature not allowed using the VP-SEM mode.

To assess the image quality of Focal CC versus both high vacuum and VP-SEM modes we first tested each method under otherwise identical imaging conditions. For each, we imaged rat brain tissue that had been heavily stained to minimize charging, at 2.5 keV. Focal CC with a chamber pressure of 5×10^{-3} mbar was compared to high vacuum and VP-SEM imaging at 0.3 mbar chamber pressure (30Pa). Images of the same brain synapse are shown (Fig. 4A-C), as well as corresponding image grey level histograms of the raw data (Fig. 4D-F). While a modest decrease in terms of the grey level intensity range was noted between the high vacuum and Focal CC images (~26%), a more substantial decrease (~56%) was clearly visible using variable pressure conditions. This is mainly due to the tremendous reduction in specimen beam current when using VP-SEM (Titze & Denk, 2013). On the Gemini SEM platform using VP-SEM at a standard 7mm working distance, we needed to increase the condenser aperture size from 30 microns to 60 microns and increase the accelerating voltage to 6.3 keV in order to reach the same specimen beam current as high vacuum (~110 pA) (data not shown).

To compare resolution and SNR of Focal CC versus high vacuum and VP-SEM modes, the same rat brain tissue sample was imaged with five different imaging parameters. First, images were collected using high vacuum, Focal CC (80% gas injection), and VP-SEM (30 Pa) with 2.5 keV and a pixel dwell time of 1 μsec (Supp. Fig. 1A-C). Then, to compensate for the reduced beam current for VP-SEM, the accelerating voltage for that method was boosted to 3.5 keV with a pixel dwell time of 2 μsec (Supp. Fig. 1D) and further to 4.0 keV with a pixel dwell time of 4 μsec (Supp. Fig. 1E). Using a Faraday cup, specimen beam current was ~110 pA at high vacuum, ~83 pA using Focal CC, and ~16 pA using VP-SEM (Supp. Fig. 2A). Increasing the accelerating voltage to 3.5 keV and then to 4.0 keV

increased the beam current for VP-SEM to ~24 pA and ~30 pA, respectively. Signal-to-noise ratio was estimated as previously described (He & Zhou, 2008, Waters, 2009) over 3 randomly chosen areas and measured at 6.13 (SD = 0.78) (high vacuum), 4.14 (0.38) (Focal CC), 0.31 (0.02) (VP-SEM), 1.67 (0.22) (VP-SEM, 3.5 keV, 2 μsec) and 2.99 (0.36) (VP-SEM, 4 keV, 4 μsec). Resolution for each mode was estimated (Supp. Fig. 2B) from 4 randomly chosen areas to be 19.9 nm (high vacuum), 20.4 nm (Focal CC), 58.4 nm (VP-SEM, 2.5 keV), 36.4 nm (VP-SEM, 3.5 keV, 2 μsec), and 30.7 nm (VP-SEM, 4.5 keV, 4 μsec dwell). Thus, in terms of both SNR and resolution, Focal CC mode performed nearly as well as high vacuum and dramatically outperformed VP-SEM using identical imaging parameters. The loss in image quality with VP-SEM could not be entirely compensated for with increased accelerating voltage or dwell time.

To evaluate the effects of Focal CC on charging, focus and stigmation, a single image frame was acquired (12k × 12k pixels, 1 μsec dwell time, ~90 second acquisition time) while repeatedly cycling the gas injection off and on using a highly charge-prone sample (lung tissue) (Fig. 5). Focal CC rapidly dissipates all charging in a matter of seconds and does not have a negative effect on instrument focus or stigmation, even when cycled off and on repeatedly. Additionally, if the gas injection was gradually halted in the middle of a run, the specimen began to massively charge and poor cutting resulted until the gas flow was restored (Supp. Movie 4).

While we have not yet conducted rigorous testing on the effect of Focal CC to allow for thinner cutting than otherwise routinely possible (<25 nm) with SBEM (Titze & Genoud, 2016), we believe this to be the case when specimen beam damage is the limiting factor and here demonstrate 20 nm cutting intervals using 10 nm pixels (Supp. Movie 4). Focal CC may facilitate this by allowing short pixel dwell times (0.5-1 μsec) and charge elimination and thus reduced specimen beam damage (Joy & Joy, 1996).

Finally, we chose to test Focal CC on specimens that were not heavily metal impregnated and thus severely charge-prone with SBEM, as are most specimens prepared for conventional transmission EM (TEM). For this purpose, we selected a legacy block of human Alzheimer's brain tissue prepared in the 1960's that was prepared with no heavy metal staining except from post-fixation with osmium tetroxide (Masliah et al., 1992; Masliah et al., 1993). Using 2.5 keV, a 4 μsec pixel dwell time, and 80% gas injection, we were able to obtain block-face images in which individual microtubules and synaptic vesicles could be resolved (Supp. Fig. 3). This is something we could not achieve using VP-SEM.

Discussion

Specimen charging is a crucial problem when it comes to SBEM, since most specimens are non-conductive due to the requirement of being embedded in epoxy resin to facilitate cutting. Modest negative surface charging results in dark streaks and black regions of the sample containing bare resin. Severe charging increases image jitter between cuts, creates intolerable image distortions, and can lead to increased specimen beam damage (Joy & Joy, 1996). While intense heavy metal *en bloc* staining can render some tissues such as brain

sufficiently conductive to be imaged under high vacuum conditions, many types of samples require variable chamber pressure to mitigate charging with a commensurate degradation of image quality and resolution due to both primary and backscatter electron scattering. Thus far the only effective solution to eliminate specimen charging in charge-prone samples while maintaining high resolution is coating of the block-face surface with a thin (1-2 nm) layer of metal between cutting cycles using an in-chamber coating system (Titze & Denk, 2013). However, this approach has a number of drawbacks, including an increase in the image acquisition time to allow for the coating process between cuts, a slight reduction in signal to noise due to the coating material itself, and the limited number of cutting, imaging and coating cycles possible before the coating materials need to be replenished.

With charge compensation by focal gas injection, a needle locally disperses nitrogen gas over the block-face surface during imaging while the chamber pressure is maintained under high vacuum conditions ($<7\times10^{-3}$ mbar). The interaction of the lower energy secondary electrons emitted from the sample surface ionizes the nitrogen gas molecules and the positive ions neutralize charging when they are attracted to and strike the sample surface (Thiel *et al.*, 1997). The spatial restriction of the low vacuum area allows the use of all types of detectors that are ordinarily used in high vacuum conditions. Furthermore, significant deterioration of image quality and a reduction of resolution by beam broadening due to electron scattering are dramatically reduced in comparison to variable pressure systems, where the entire chamber is at low vacuum and the interaction volume of the primary and backscattered electrons is much larger (Mathieu, 1999). The addition of focal gas injection does not affect the data acquisition time with SBEM, and in fact can reduce it by allowing for shorter pixel dwell times due to the improvement in SNR. Indeed, even when increasing the accelerating voltage from 2.5 to 4.0 keV (60%) and increasing the pixel dwell time from 1 μsec to 4 μsec (4×), SNR was ~28% lower using VP-SEM than Focal CC, and the resolution obtainable by Focal CC was nearly the same as measured using high vacuum.

Unlike FIB-SEM, one of the main limitations in cutting at very thin intervals (<25nm) with SBEM is beam induced damage to the embedding resin (Titze & Genoud, 2016), and thus any approach that reduces this by shortening pixel dwell times as does Focal CC should improve thin cutting (Supp. Movie 4). Additionally, it is known that specimen charging can increase beam damage to the specimen due to lowering of the primary beam landing energy by electrostatic repulsion, since lower energy electrons (i.e. 1 keV) are significantly more damaging to specimens than higher energy electrons (i.e. 10 keV) (Joy & Joy, 1996).

Finally, we tested Focal CC on a sample prepared for conventional TEM using only osmium tetroxide post-fixation to generate contrast and found it possible to resolve individual microtubules and synaptic vesicles (Supp. Figure 3), opening the possibility of using any previously existing TEM specimens for SBEM with greatly improved results.

We find Focal CC to be one of the most effective means of mitigating block-face charging while maintaining high-resolution. Indeed, here we show data from epoxy resin embedded samples that are highly charge-prone but can easily be imaged using this method. The system we describe is easy to install on existing SBEM platforms, is inexpensive, extremely simple and reliable and does not negatively affect the stability or other operational aspects of

the SBEM and does not increase image acquisition time. We anticipate that, given the dramatic benefits of Focal CC, this approach will become widely adopted by those performing serial block-face scanning EM.

Supplementary Material

Refer to Web version on PubMed Central for supplementary material.

Acknowledgments

We gratefully acknowledge the contributions of Zeiss in providing the gas injection hardware we modified to enable this work and to helpful discussions regarding adaptation of this to operate on both their variable pressure and UHV platforms. We thank Mason Mackey and Andrea Thor for assistance with specimen preparation, Junru Hu for cell culturing, and Sebastien Phan and Hiroyuki Hakozaki for expert technical assistance and advice. This work was supported by a grant from the NIH National Institute of General Medical Sciences under award number P41GM103412 to Mark H. Ellisman, which partially supports the National Center for Microscopy and Imaging Research.

References

Bouwer JC, Deerinck TJ, Bushong E, Astakhov V, Ramachandra R, Peltier ST, Ellisman MH. Deceleration of probe beam by stage bias potential improves resolution of serial block-face scanning electron microscopic images. Adv Struct Chem Imaging. 2017; 2:11. [PubMed: 27695667]

Deerinck TJ, Bushong EA, Lev-Ram V, Shu X, Tsien RY, Ellisman MH. Enhancing serial block-face scanning electron microscopy to enable high resolution 3-D nanohistology of cells and tissues. Microsc Microanal. 2010; 16:1138–1139.

Denk W, Horstmann H. Serial block-face scanning electron microscopy to reconstruct three-dimensional tissue nanostructure. PLoS Biol. 2004; 2:e329. [PubMed: 15514700]

Friedman PL, Ellisman MH. Enhanced visualization of peripheral nerve and sensory receptors in the scanning electron microscope using cryofracture and osmium-thiocarbohydrazideosmium impregnation. J Neurocytol. 1981; 10:111–131. [PubMed: 7310442]

Griffin BJ. Variable pressure and environmental scanning electron microscopy: imaging of biological samples. Methods Mol Biol. 2007; 369:467–495. [PubMed: 17656765]

He ZJ, Zhou JZ. Empirical evaluation of a new method for calculating signal-to-noise ratio for microarray data analysis. Appl Environ Microb. 2008; 74:2957–2966.

Joy DC, Joy CS. Low voltage scanning electron microscopy. Micron. 1996; 27:247–263.

Joy DC, Ko YU, Hwu JJ. Metrics of resolution and performance for CD-SEMs. P Soc Photo-Opt Ins. 2000; 3998:108–114.

Leighton SB. SEM images of block faces, cut by a miniature microtome within the SEM - a technical note. Scan Electron Microsc. 1981:73–76.

Martell JD, Deerinck TJ, Sancak Y, Poulos TL, Mootha VK, Sosinsky GE, Ellisman MH, Ting AY. Engineered ascorbate peroxidase as a genetically encoded reporter for electron microscopy. Nat Biotechnol. 2012; 30:1143–1148. [PubMed: 23086203]

Masliah E, Ellisman M, Carragher B, Mallory M, Young S, Hansen L, DeTeresa R, Terry RD. Three-dimensional analysis of the relationship between synaptic pathology and neuropil threads in Alzheimer disease. Journal of Neuropathology & Experimental Neurology. 1992; 51:404–414. [PubMed: 1619440]

Masliah E, Mallory M, Deerinck T, Deteresa R, Lamont S, Miller A, Terry RD, Carragher B, Ellisman M. Re-evaluation of the structural organization of neuritic plaques in Alzheimer's disease. Journal of Neuropathology & Experimental Neurology. 1993; 52:619–632. [PubMed: 8229081]

Mathieu C. The beam-gas and signal-gas interactions in the variable pressure scanning electron microscope. Scanning Microsc. 1999; 13:23–41.

Murakami T, Iida N, Taguchi T, Ohtani O, Kikuta A, Ohtsuka A, Itoshima T. Conductive staining of biological specimens for scanning electron microscopy with special reference to ligand-mediated osmium impregnation. Scan Electron Microsc. 1983; Pt 1:235–246.

Ngo JT, Adams SR, Deerinck TJ, Boassa D, Rodriguez-Rivera F, Palida SF, Bertozzi CR, Ellisman MH, Tsien RY. Click-EM for imaging metabolically tagged nonprotein biomolecules. Nat Chem Biol. 2016; 12:459–465. [PubMed: 27110681]

Nguyen HB, Thai TQ, Saitoh S, Wu B, Saitoh Y, Shimo S, Fujitani H, Otobe H, Ohno N. Conductive resins improve charging and resolution of acquired images in electron microscopic volume imaging. Sci Rep. 2016; 6:23721. [PubMed: 27020327]

Thiel BL, Bache IC, Fletcher AL, Meredith P, Donald AM. An improved model for gaseous amplification in the environmental SEM. J Microsc. 1997; 187:143–157.

Titze B, Denk W. Automated in-chamber specimen coating for serial block-face electron microscopy. J Microsc. 2013; 250:101–110. [PubMed: 23451833]

Titze B, Genoud C. Volume scanning electron microscopy for imaging biological ultrastructure. Biol Cell. 2016; 108:307–323. [PubMed: 27432264]

Wanner AA, Genoud C, Friedrich RW. 3-dimensional electron microscopic imaging of the zebrafish olfactory bulb and dense reconstruction of neurons. Sci Data. 2016; 3:160100. [PubMed: 27824337]

Waters JC. Accuracy and precision in quantitative fluorescence microscopy. J Cell Biol. 2009; 185(7): 1135–1148. [PubMed: 19564400]

Wilke SA, Antonios JK, Bushong EA, Badkoobehi A, Malek E, Hwang M, Terada M, Ellisman MH, Ghosh A. Deconstructing complexity: serial block-face electron microscopic analysis of the hippocampal mossy fiber synapse. J Neurosci. 2013; 33:507–522. [PubMed: 23303931]

Williams ME, Wilke SA, Daggett A, Davis E, Otto S, Ravi D, Ripley B, Bushong EA, Ellisman MH, Klein G, Ghosh A. Cadherin-9 regulates synapse-specific differentiation in the developing hippocampus. Neuron. 2011; 71:640–655. [PubMed: 21867881]

Lay Description

Serial block-face scanning electron microscopy is rapidly becoming the method of choice for obtaining 3-dimensional volume imaging data of cells and tissues at nanometer-scale resolution. However, one of the main drawbacks of this approach is the problem of specimen charging of the non-conductive epoxy resin used to embed specimens, causing moderate to severe image distortions. The most common method used to mitigate specimen charging is the use of variable-pressure SEM, in which the entire specimen chamber is held at low vacuum (typically 0.1-0.5 mbar) and the residual gas molecules are ionized, mainly by secondary electrons emitted from the sample surface, and the resulting ions are attracted to and neutralize specimen charge. This approach, while effective, results in signal loss and resolution degradation due to electron scattering caused by the large number of gas molecules present in the entire specimen chamber. Here we describe a simple device that enables a very small, localized stream of gas to be injected directly over the specimen surface during imaging while maintaining the chamber at high vacuum ($<7\times10^{-3}$ mbar). While the gas ionization charge neutralization is similar to variable pressure SEM, electron scattering is greatly reduced, resulting in a significant improvement in signal-to-noise and resolution. The key to making this method work with serial block-face scanning electron microscopy was development of a device that allows the precise positioning of the small stream of gas to the very small space between the backscatter detector and the specimen block; a space which must also be occupied by the ultramicrotome arm in a different part of the imaging cycle. The nozzle composition and mechanism for precise repositioning required special design considerations and is described below. The resulting device and local gas injection method allows for high-resolution imaging of even the most charge-prone samples by serial block-face scanning electron microscopy.

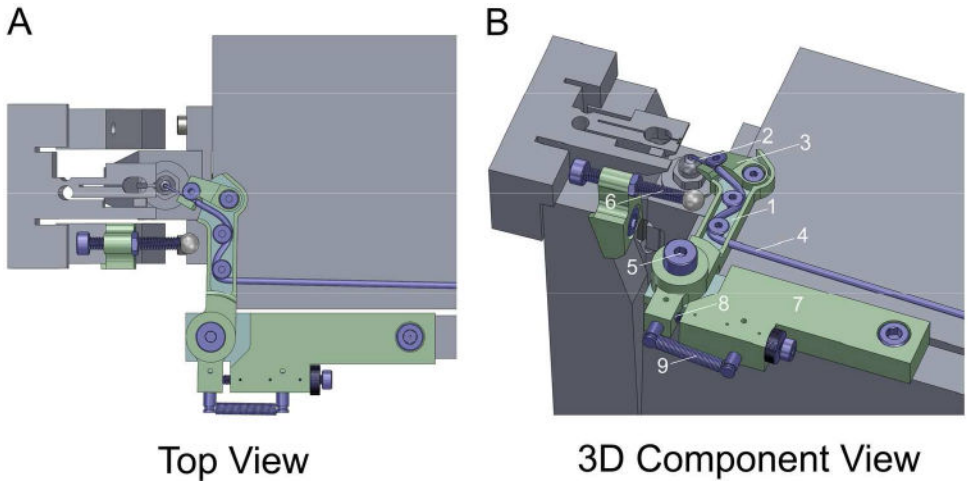

Figure 1.

CAD renderings depicting A) a top view of the 3View ultramicrotome with Focal CC assembly attached and nozzle positioned for gas delivery (Focal CC components shown in green and blue), and B) a 3D view with Focal CC assembly components identified as follows: 1) rotating arm, 2) rigid needle, 3) ramped platform, 4) silicon tubing, 5) shoulder screw/bushing comprising primary bearing, 6) adjustable tappet, 7) mounting block, 8) adjustable stop, and 9) extension spring.

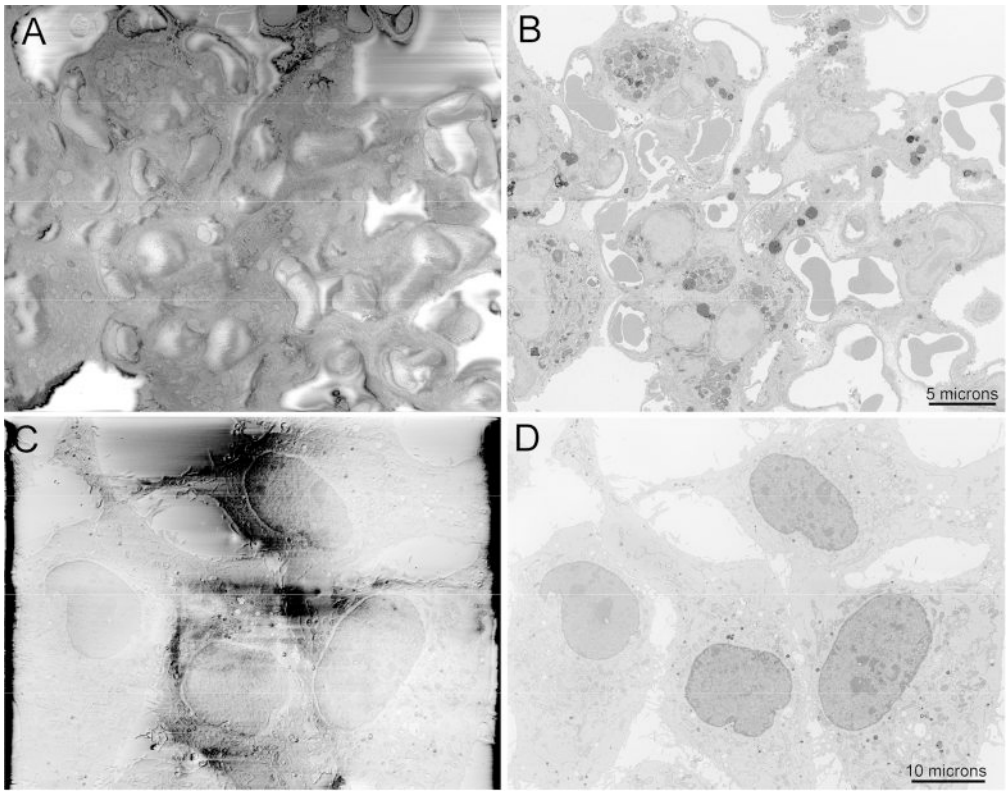

Figure 2.

Block-face imaging of charge-prone samples of A) lung tissue and C) a cell culture monolayer with DNA stained and imaged at high vacuum, both showing major specimen charging artifacts. B and D) Complete abrogation of specimen charging of the same fields of view by focal nitrogen gas injection. Bars = 5 and 10 microns.

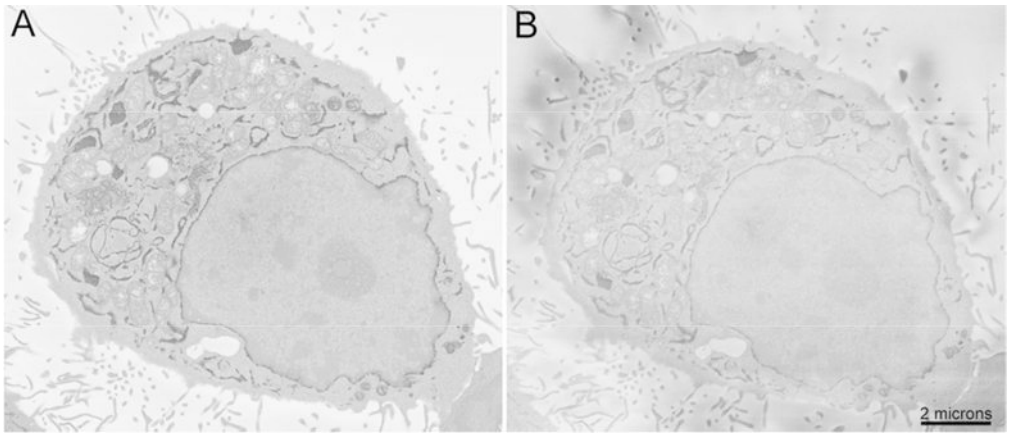

Figure 3.

Direct comparison of charge compensation (A) and variable pressure SEM (B) of the same cultured cell expressing APEX2 targeted to the endomembrane system by KDEL. Gas injection was 80% N_2 and chamber pressure was ~5×10^{-3} mbar. VP-SEM was 0.3 mbar chamber pressure (maximum pressure allowed using Gemini SEM) using N_2 with otherwise identical imaging conditions (2.5 keV and 1 μsec pixel dwell time). Bar = 2 microns.

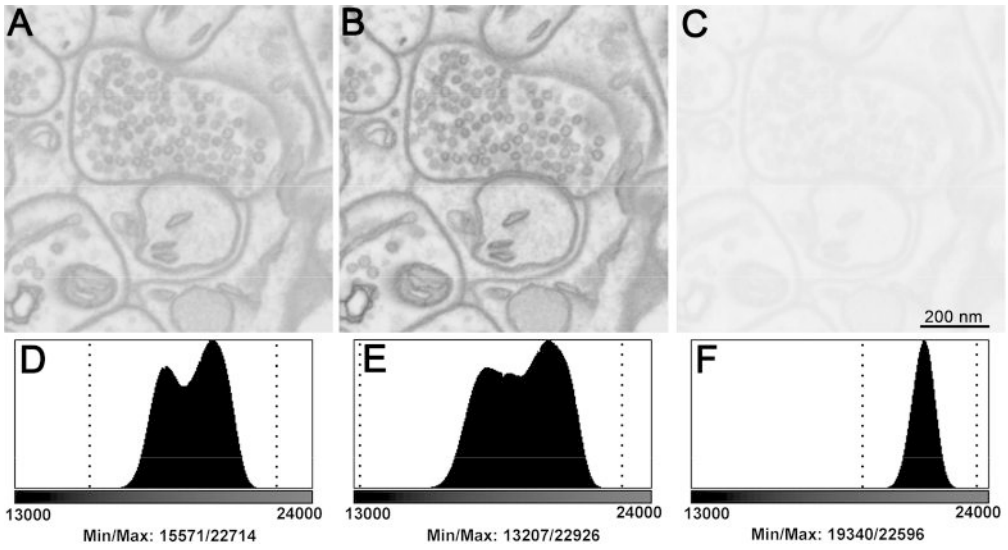

Figure 4.

Raw unadjusted images comparing block-face imaging of the same brain synapse A) using Focal CC, B) under high vacuum and C) using variable pressure imaging at 0.3 mbar chamber pressure. All other instrument conditions were kept identical in order to gauge effects on image grey level intensity ranges. There is a substantial loss in the grey level intensity range using variable pressure (56.2%) compared to high vacuum and focal gas injection. Histograms (D-F) of each image reveal significant loss of grey level intensity range. Minimum/maximum pixel values are denoted by vertical dotted lines: D: 15571/22714, E: 13207/22926 and F: 19340/22596. Bar = 200 nm.

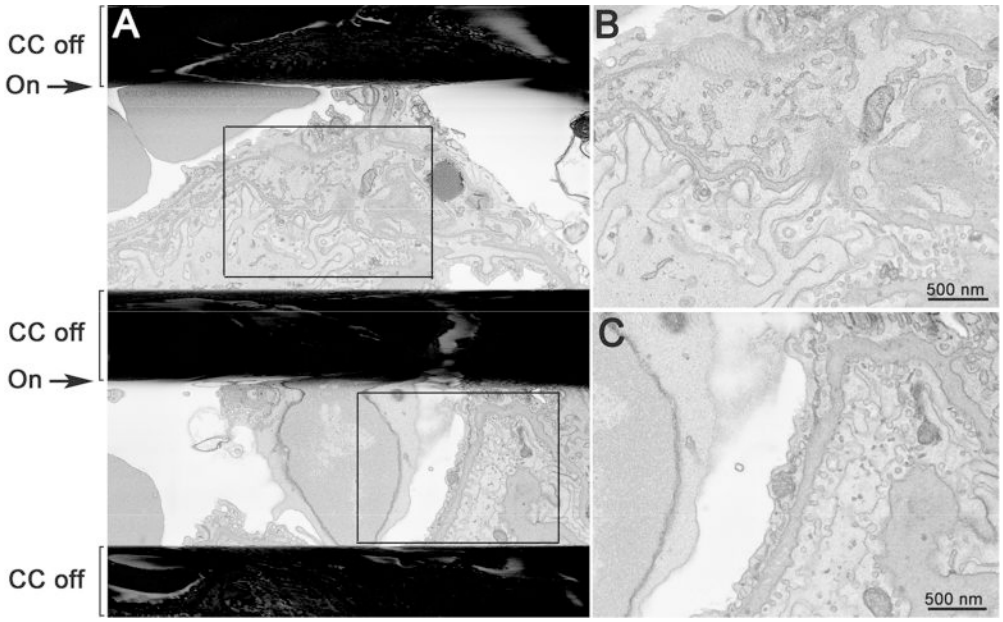

Figure 5.

A) Image of lung tissue in which Focal CC was repeatedly cycled off and on during a single continuous frame acquisition (~90 seconds) showing rapid and complete charge elimination and no residual effect of gas injection on focus or stigmation. The black horizontal bands represent massive charging that occurs with the gas cycled off. B and C are enlargements of the boxed regions in A. Bars = 500 nm.